




Circumferential wrinkling of polymer nanofibers

Mojtaba Ahmadi , Oksana Zholobko , and Xiang-Fa Wu *

Department of Mechanical Engineering, North Dakota State University, Fargo, North Dakota, 58108-6050, USA



(Received 21 January 2020; accepted 9 June 2020; published 1 July 2020)

Surface wrinkles are commonly observed in soft polymer nanofibers produced in electrospinning. This paper studies the conditions of circumferential wrinkling in polymer nanofibers under axial stretching. A nonlinear continuum mechanics model is formulated to take into account the combined effects of surface energy and nonlinear elasticity of the nanofibers on wrinkling initiation, in which the soft nanofibers are treated as incompressible, isotropically hyperelastic neo-Hookean solid. The critical condition to trigger circumferential wrinkling is determined and its dependencies upon the surface energy, mechanical properties, and geometries of the nanofibers are examined. In the limiting case of spontaneous circumferential wrinkling, the theoretical minimum radius of soft nanofibers producible in electrospinning is determined, which is related closely to the intrinsic length $l_0 = \gamma/E$ of the polymer (γ : the surface energy; E : a measure of the elastic modulus), and compared with that of spontaneous longitudinal wrinkling in polymer nanofibers. The present study provides a rational understanding of surface wrinkling in polymer nanofibers and a technical approach for actively tuning the surface morphologies of polymer nanofibers for applications, e.g., high-grade filtration, oil-water separation, tissue scaffolding, etc.

DOI: [10.1103/PhysRevE.102.013001](https://doi.org/10.1103/PhysRevE.102.013001)

I. INTRODUCTION

With development of electrospinning and solution and melt blowing techniques, ultrathin continuous polymer fibers with diameters in the range of a few microns down to nanometers can be produced in a low-cost and well scalable way [1–4]. Due to their high surface area to volume ratio, improved tensile strength, and tailorable surface morphology and microstructures, electrospun continuous nanofibers of natural and synthetic polymers and polymer-derived carbon, silicon, metals, metal oxides, ceramics, etc., have been considered as a new class of nanostructured materials for broad structural and multifunctional applications under intensive investigations. These unique properties of nanofibrous materials result mainly from their size effects in their mechanical, physical, and chemical properties. So far, electrospun nanofibrous materials have been considered as the important constituents in various emerging applications such as protective clothing and wound dressing [5–7]; ultrafine gas and liquid filtration [8–12]; nanofiber-reinforced composites [13–19]; biodegradable tissue scaffolds [20–23]; drug delivery [24–28]; and energy harvesting, conversion, and storage [29–35], among others. This has triggered rapidly expanding research on the electrospinning process and electrospinnability of various polymer solutions [36–43], mechanical characterization of nanofibers and nanofiber membranes (e.g., elastic modulus, tensile strength, plasticity, etc.) [44–55], and modeling of the mechanical behaviors of nanofibers and fiber networks [56–64], etc.

In a typical electrospinning process as illustrated in Fig. 1, a polymer solution is fed into a capillary tube to form a droplet

at the capillary tip. Under the action of a high-voltage direct current (dc) electrostatic field, the droplet deforms into a Taylor cone [4,36,65,66]. Once the electrostatic force overcomes the surface tension of the Taylor cone, the droplet is ejected and elongated into an electrospinning jet. After a variety of jet instabilities [4,36,66–69], solvent evaporation [70,71], and polymer solidification, the drying jet is finally collected as a nonwoven nanofiber mat on the collector. The entire process of electrospinning is a multiphysics process involving electrohydrodynamics, heat and mass transfer, phase separation, polymer solidification, etc. The fast solvent evaporation from the tiny jet may unavoidably induce the radial gradient in the material properties, microstructures (e.g., polymer chain orientation), and residual stresses and strains in the resulting fiber cross section though experimental evidence is still lacking at this time. In the electrospinning process, production of continuous nanofibers with controllable surface morphology is a desirable technological strategy to realize many promising applications of nanofibers such as gas and liquid filtration and tissue scaffolding. Typically, a dilute polymer solution made from a soft polymer dissolved in a highly volatile organic solvent will lead to porous and wrinkled surfaces due to fast drying induced polymer-solvent phase separation and nonuniform residual strains across the fiber section. Figure 2 shows the electron scanning microscopy (SEM) micrographs of circumferential surface wrinkles on electrospun polystyrene (PS) nanofibers produced by electrospinning a 10 wt% PS-dimethylformamide (DMF) solution. To date, substantial experimental and modeling approaches have been made to understand and control the surface wrinkling in electrospun nanofibers.

Theoretically, Wu *et al.* [61] and Wu [62] formulated a nonlinear elasticity model to explore the physical mechanisms governing the longitudinal wrinkling in soft nanofibers under

*Xiangfa.Wu@ndsu.edu

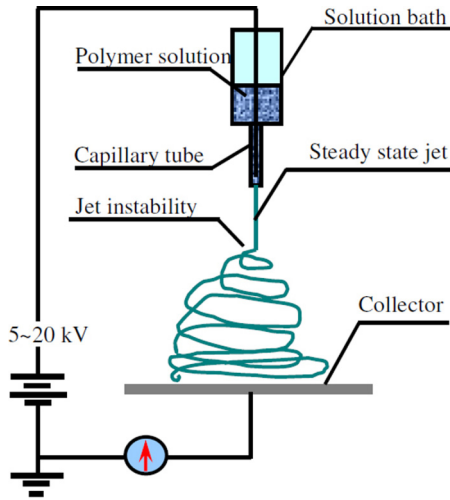


FIG. 1. Schematic electrospinning process.

axial stretching, which was discovered in single-nanofiber tension tests [54,55]. The main contribution of these works is that surface energy as a unique physical parameter of nanostructured materials was introduced in wrinkling analysis of soft nanofibers and discovery of spontaneous wrinkling of soft nanofibers when the fiber radius is below a certain value. Such a threshold fiber radius is a function with respect to the surface energy and elastic properties of the nanofibers and is independent of the electrospinning process and process parameters. Due to the unique spontaneous wrinkling at small fiber radii, electrospinning is unable to fabricate continuous nanofibers below a certain fiber radius because of jet-beading instability. In parallel, Mora *et al.* [72] and Taffetani and Ciarletta [73] conducted an experimental study to show the Rayleigh-Plateau instability in slender gel cylinders and formulated the first-principle models to address their observations by means of linear perturbations within the framework of small deformations. The critical condition [72] to trigger such a longitudinal surface instability (beading) was determined as $\gamma = 6\mu\rho$, where γ , μ , and ρ are the surface tension, shear modulus, and initial radius of the gel cylinder, respectively.

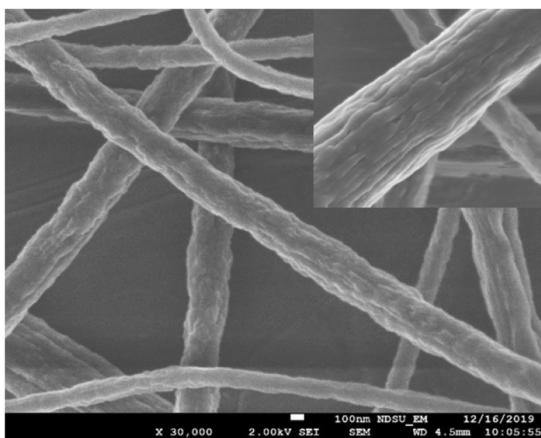


FIG. 2. SEM micrographs of circumferential wrinkles on PS nanofibers prepared by electrospinning a 10 wt% PS-DMF solution.

This critical condition is similar to one to evoke spontaneous longitudinal rippling in soft nanofibers under axial stretching [61,62] though the latter were based on a hyperelastic solid model for rubbery polymeric materials. Furthermore, Taffetani and Ciarletta [74] and Ciarletta *et al.* [75] formulated a systematic nonlinear elastic framework to investigate the effect of capillary energy on beading instability in soft cylindrical gels, a phenomenon similar to longitudinal rippling in soft nanofibers under axial stretching [61]. Sophisticated linear and nonlinear instability analyses were conducted in these studies while the effect of axial stretching as a common physical condition in practice was excluded in these studies; thus it is difficult to apply these theoretical results to guide practical applications in materials science and other engineering fields such as nanofiber fabrication, single-fiber tensile test, etc. In addition, by using the finite element method, Pai *et al.* [76] and Ahmadi and Wu [77] conducted systematic simulations of nanofiber wrinkling to identify the correlation of critical strain to the corresponding circumferential wrinkle mode of core-shell nanofibers at varying fiber geometries and elastic properties as observed in experiments. The simulation results can be utilized for active wrinkling control for desired surface morphologies in fiber fabrication and applications. Yet, these models did not take into account the effects of surface energy on the wrinkling behavior of these soft polymer fibers.

In the practice of electrospinning, circumferential wrinkling is commonly observed in soft electrospun nanofibers. Yet, no theoretical modeling study has been reported yet in the literature on exploring the rational mechanisms of such surface instability in electrospun nanofibers, such as the effect of surface energy and the threshold fiber diameter to trigger spontaneous circumferential wrinkling. Therefore, this paper aims to explore the critical condition to trigger circumferential wrinkling in polymer nanofibers under axial stretching. After a brief introduction above, the rest of the paper is arranged as follows. Section II formulates the nonlinear elasticity model to take into account the nonlinear elasticity, surface energy, and axial stretch of the soft nanofibers. As a simple approach to understanding the surface instability, the soft nanofibers are treated as an incompressible, isotropic, hyperelastic neo-Hookean solid, and the wrinkling condition is obtained via mathematical perturbation on the basis of the first principle of the nanofiber system. Section III conducts detailed numerical scaling analysis to demonstrate the correlation of critical axial stretch to the corresponding circumferential wrinkle mode. The threshold fiber radius to trigger the spontaneous circumferential wrinkling is determined in the limiting case of zero axial stretch. In consequence, concluding remarks of the present study are made in Sec. IV.

II. MODEL DEVELOPMENT

Consider a soft polymer nanofiber at its undisturbed stretch-free state as a thin, perfectly circular cylinder with the initial radius R_0 . As mentioned above, the fast solvent evaporation in a thin polymer-solution jet during electrospinning may unavoidably induce the radial gradients of the material properties, microstructures, and residual stresses and strains in the nanofiber cross section. However, it is reasonable to

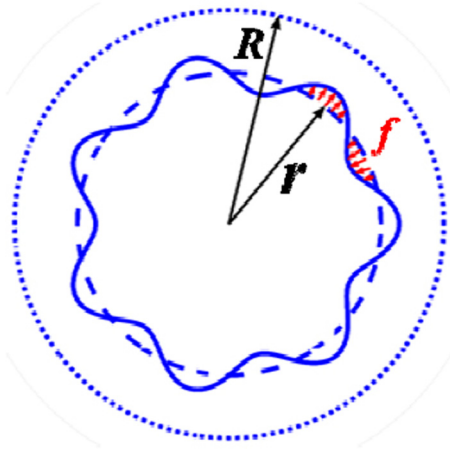


FIG. 3. Coordinate systems of the undisturbed stretch-free configuration (R, Θ, Z), prestretched configuration (r, θ, z) without wrinkles, and current configuration ($\tilde{r}, \tilde{\theta}, \tilde{z}$) with circumferential wrinkles.

consider these gradients as the secondary effects and assume the soft polymeric material of the fiber as an incompressible, isotropic, hyperelastic neo-Hookean solid. For the convenience of the discussion hereafter, three configurations are introduced to define the motion of a material point inside the fiber as shown in Fig. 3:

- (1) Undisturbed stretch-free configuration (with surface tension ignored) (R, Θ, Z);
- (2) Prestretched configuration (with surface tension) (r, θ, z);
- (3) Current configuration (with circumferential wrinkles) ($\tilde{r}, \tilde{\theta}, \tilde{z}$).

In the following, the critical condition to trigger circumferential wrinkling is to be determined via linear perturbation of the elastic solution to the prestretched state of the soft polymer nanofiber in the current configuration.

A. Thin soft polymer nanofiber under axial prestretching

In the prestretched configuration, the soft polymer nanofiber is assumed under action of uniform axial stretching, and the solution to an axisymmetric deformation of the nanofiber can be expressed as [58,61]

$$\begin{aligned} r &= \lambda_1 R \quad (0 \leq R \leq R_0), \quad \theta = \Theta \quad (0 \leq \Theta \leq 2\pi), \\ z &= \lambda_3 Z \quad (-\infty \leq Z \leq +\infty), \end{aligned} \quad (1)$$

where λ_1 and λ_3 are the transverse and longitudinal stretches, respectively. The above deformation has the deformation gradient

$$\mathbf{F} = \begin{bmatrix} \frac{\partial r}{\partial R} & \frac{\partial r}{R\partial\Theta} & \frac{\partial r}{\partial Z} \\ r\frac{\partial\theta}{\partial R} & r\frac{\partial\theta}{R\partial\Theta} & r\frac{\partial\theta}{\partial Z} \\ \frac{\partial z}{\partial R} & \frac{\partial z}{R\partial\Theta} & \frac{\partial z}{\partial Z} \end{bmatrix} = \begin{bmatrix} \lambda_1 & 0 & 0 \\ 0 & \lambda_1 & 0 \\ 0 & 0 & \lambda_3 \end{bmatrix}. \quad (2)$$

Material incompressibility of the polymer fiber gives the geometrical constraint of λ_1 and λ_3 :

$$\lambda_1^2 \lambda_3 = 1. \quad (3)$$

With the above deformations, the corresponding left Cauchy-Green tensor \mathbf{B} is

$$\mathbf{B} = \mathbf{F}\mathbf{F}^T = \begin{bmatrix} \lambda_1^2 & 0 & 0 \\ 0 & \lambda_1^2 & 0 \\ 0 & 0 & \lambda_3^2 \end{bmatrix}. \quad (4)$$

The three principal scalar invariants of \mathbf{B} are

$$I_1 = 2\lambda_1^2 + \lambda_3^2 = 2\lambda_3^{-1} + \lambda_3^2, \quad I_2 = 2\lambda_3 + \lambda_3^{-2}, \quad I_3 = 1. \quad (5)$$

In the present case, the soft nanofiber is treated as an incompressible, isotropic, hyperelastic neo-Hookean solid. Its constitutive relationship can be expressed in terms of Cauchy stress tensor \mathbf{T} versus the left Cauchy-Green tensor \mathbf{B} as

$$\mathbf{T} = -p\mathbf{I} + 2c_1\mathbf{B}, \quad (6)$$

where p is the unknown hydrostatic pressure to be determined, and c_1 is a material constant. The stress tensor (6) can be further expressed in terms of stress components:

$$T_{rr} = T_{\theta\theta} = -p + 2c_1\lambda_1^2 = -p + 2c_1\lambda_3^{-1}, \quad (7)$$

$$T_{zz} = -p + 2c_1\lambda_3^2, \quad (8)$$

$$T_{r\theta} = T_{rz} = T_{\theta z} = 0. \quad (9)$$

In terms of cylindrical coordinates, equilibrium equations of the axisymmetric fiber under uniform axial tension are

$$\frac{\partial T_{rr}}{\partial r} + \frac{T_{rr} - T_{\theta\theta}}{r} = 0, \quad (10)$$

$$\frac{\partial T_{\theta\theta}}{\partial \theta} = 0, \quad (11)$$

$$\frac{\partial T_{zz}}{\partial z} = 0. \quad (12)$$

In the above, two traction boundary conditions (BCs) are triggered at the fiber surface and along the fiber axis. In addition, surface tension produces a uniform radial compressive stress at the fiber surface as

$$T_{rr} = -\frac{\gamma}{r_0}, \quad (13)$$

where γ (N/m) is surface tension (surface energy) of the amorphous polymeric material and is assumed to be independent of the axial stretch and fiber radius, and r_0 is the fiber radius after deformation in the current configuration. Moreover, force equilibrium along the fiber axis can be cast as

$$P = 2\pi \int_0^{r_0} r T_{zz} dr + 2\pi r_0 \gamma, \quad (14)$$

where P is the resultant of the external axial tensile force. By solving (10)–(12) under traction conditions (13) and (14), the axial stress of the soft polymer nanofiber can be determined as

$$\frac{\sigma}{c_1} = \frac{P}{\pi r_0^2 c_1} = 2 \left(\lambda_3^2 - \frac{1}{\lambda_3} \right) + \frac{l_0}{r_0}, \quad (15)$$

where $l_0 = \gamma/c_1$ is the intrinsic length of the polymeric material. Equation (15) can be further arranged as a function of the undisturbed radius of a stretch-free fiber (with surface tension ignored) by applying the deformation relation $r_0 = \lambda_1 R_0 = R_0 \lambda_3^{-1/2}$ as

$$\frac{\sigma}{c_1} = \frac{P}{\pi R_0^2 c_1} = 2 \left(\lambda_3 - \frac{1}{\lambda_3^2} \right) + \frac{l_0}{R_0} \frac{1}{\sqrt{\lambda_3}}. \quad (16)$$

It can be concluded from the above derivations that under uniaxial tensile stress and surface tension, a soft nanofiber is in the triaxial stress state, and its three principal stress components at a material point are independent of the radial position of the fiber. Similar derivations have been considered in our previous studies of longitudinal wrinkling and wave propagation in soft polymer nanofibers [61,62].

B. Circumferential wrinkling of a soft polymer nanofiber under axial stretching

Now let us consider the circumferential wrinkling deformation of a soft polymer nanofiber under uniform axial stretching as a small disturbance superimposed onto the elastic solution to the prestretched nanofiber as determined in Sec. II A. After the wrinkling initiation on the nanofiber, a simple approach is to assume the coordinates of a material point in the current configuration as

$$\begin{aligned} \tilde{r} &= [\lambda_1 + f(\Theta)]R \quad (0 \leq R \leq R_0), \\ \tilde{\theta} &= \Theta + g(\Theta) \quad (0 \leq \Theta \leq 2\pi), \\ \tilde{z} &= \lambda_3 Z \quad (-\infty \leq Z \leq +\infty), \end{aligned} \quad (17)$$

where $f(\Theta)$ and $g(\Theta)$ are two small unknown disturbance functions satisfying BCs (13) and (14). It needs to be mentioned that the choice of (17) belongs to one of the simplest possible incremental solutions of the present surface instability problem to avoid lengthy mathematical derivations based on more general assumption of the possible displacement solutions as commonly used in nonlinear analysis of elastic instability [74,75] while it can lead to practical, physically meaningful solutions. Thus, the corresponding deformation gradient matrix $\tilde{\mathbf{F}}$ and left Cauchy-Green tensor $\tilde{\mathbf{B}}$ are

$$\tilde{\mathbf{F}} = \begin{bmatrix} \lambda_1 + f & f_\Theta & 0 \\ 0 & (\lambda_1 + f)(1 + g_\Theta) & 0 \\ 0 & 0 & \lambda_3 \end{bmatrix}, \quad (18)$$

$$\begin{aligned} \tilde{\mathbf{B}} &= \tilde{\mathbf{F}}\tilde{\mathbf{F}}^T \\ &= \begin{bmatrix} (\lambda_1 + f)^2 + f_\Theta^2 & (\lambda_1 + f)(1 + g_\Theta)f_\Theta & 0 \\ (\lambda_1 + f)(1 + g_\Theta)f_\Theta & (\lambda_1 + f)^2(1 + g_\Theta)^2 & 0 \\ 0 & 0 & \lambda_3^2 \end{bmatrix}, \end{aligned} \quad (19)$$

where f_Θ and g_Θ are derivatives of $f(\Theta)$ and $g(\Theta)$ with respect to Θ .

The scalar invariants of $\tilde{\mathbf{B}}$ above are

$$I_1 = (\lambda_1 + f)^2 + f_\Theta^2 + (\lambda_1 + f)^2(1 + g_\Theta)^2 + \lambda_3^2, \quad (20)$$

$$\begin{aligned} I_2 &= \frac{1}{2} [(\lambda_1 + f)^2 + f_\Theta^2 + (\lambda_1 + f)^2(1 + g_\Theta)^2 + \lambda_3^2]^2 \\ &\quad - \frac{1}{2} [(\lambda_1 + f)^2 + f_\Theta^2]^2 - \frac{1}{2} (\lambda_1 + f)^4 (1 + g_\Theta)^4 \\ &\quad - (\lambda_1 + f)^2 (1 + g_\Theta)^2 f_\Theta^2 - \frac{1}{2} \lambda_3^4, \end{aligned} \quad (21)$$

$$I_3 = \lambda_3^2 (\lambda_1 + f)^4 (1 + g_\Theta)^2. \quad (22)$$

Material incompressibility of the polymer nanofiber in this state is

$$\det(\tilde{\mathbf{B}}) = 1, \quad (23)$$

which results in

$$\lambda_3 (\lambda_1 + f)^2 (1 + g_\Theta) = 1. \quad (24)$$

The strain energy density for an incompressible, isotropic, hyperelastic neo-Hookean solid is

$$e = \mu(I_1 - 3), \quad (25)$$

where I_1 is the first principal invariant of $\tilde{\mathbf{B}}$, and μ is the shear modulus of the neo-Hookean solid as given in (6). Hence, the potential energy functional Π of the soft polymer nanofiber under uniaxial axial stretching and surface tension has the form

$$\Pi = \iiint e \tilde{r} d\tilde{\theta} d\tilde{r} d\tilde{z} + \iint \gamma \sqrt{\tilde{r}^2 + \tilde{r}_\theta^2} d\tilde{\theta} d\tilde{z} - \int P d(\tilde{z} - Z), \quad (26)$$

which can be expressed in terms of the coordinates defined in the configuration of the undisturbed stretch-free fiber as

$$\Pi = \frac{1}{2} R_0^2 Z \int_\Theta e d\Theta + R_0 Z \int_\Theta \frac{\gamma}{\lambda_1 + f} d\Theta - P Z (\lambda_3 - 1), \quad (27)$$

where the higher-order terms in the second integral of the surface energy have been ignored. By substituting (20)–(25) into (27), applying the functional variation on (27), evoking the material incompressibility (3), and finally ignoring the higher-order terms, a standard second-order linear ordinary differential equation (ODE) of constant coefficients can be obtained as

$$R_0 \mu \lambda_3^{1/2} f_{\Theta\Theta} - R_0 \left(4\mu \lambda_3^{1/2} - \frac{\gamma}{R_0} \lambda_3^2 \right) f + \gamma \lambda_3^{3/2} = 0. \quad (28)$$

Equation (28) indicates that the condition to trigger circumferential wrinkling on a soft polymer nanofiber under uniform axial stretching is governed by the material elasticity, surface energy, initial fiber radius, and axial stretch of the nanofiber. Furthermore, Eq. (28) can be recast as

$$A f_{\Theta\Theta} + B f + C = 0, \quad (29)$$

where coefficients A , B , and C can be related to the material elasticity, surface energy, applied prestretch, and fiber geometry (radius):

$$A = R_0 \mu \lambda_3^{1/2}, \quad (30)$$

$$B = -R_0 \left(4\mu \lambda_3^{1/2} - \frac{\gamma}{R_0} \lambda_3^2 \right), \quad (31)$$

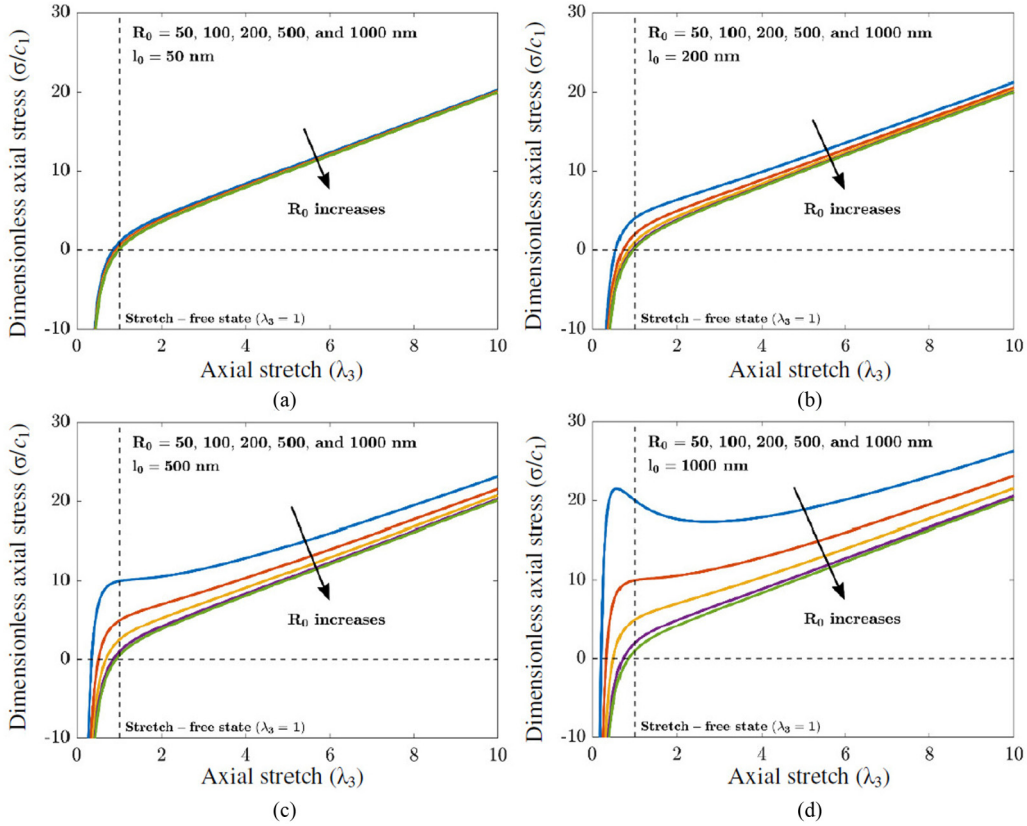


FIG. 4. Variation of the dimensionless axial stress of prestretched soft nanofibers with respect to the axial stretch λ_3 at four initial fiber radii and four intrinsic lengths (R_0 and $l_0 = 50, 200, 500,$ and 1000 nm, respectively).

$$C = \gamma \lambda_3^{3/2}. \quad (32)$$

Surface wrinkling on a soft polymer nanofiber can be determined by seeking periodic solutions to homogeneous equation (29) as

$$A f_{\Theta\Theta} + B f = 0. \quad (33)$$

Consider a periodic solution to (33) along the circumference with respect to Θ as

$$f(\Theta) = A_0 \exp(ik\Theta), \quad (34)$$

where A_0 is the complex amplitude of surface disturbance, and k is the wave number of the wrinkles. Consequently, by substituting (34) into (33) the wave number k can be determined as

$$k = \sqrt{B/A}, \quad (35)$$

which is a positive number to ensure a physically meaningful circumferential wrinkle on the fiber surface. Therefore, the condition of surface wrinkling on soft rubbery polymer nanofibers is

$$B/A > 0, \quad (36)$$

which can be expressed in terms of material properties μ and γ , geometry R_0 , and longitudinal stretch λ_3 as

$$\frac{R_0}{\lambda_3^{3/2}} < \frac{\gamma}{4\mu}. \quad (37)$$

Relation (37) elucidates the scaling properties among initial fiber radius, material properties, and axial stretch for circumferential wrinkling of soft polymer nanofibers under axial stretching.

III. NUMERICAL EXAMPLES AND DISCUSSIONS

A. Axial stress of prestretched soft polymer nanofibers

In the cases of the intrinsic length taking $l_0 = 50, 200, 500,$ and 1000 nm and the initial fiber radius taking $R_0 = 50, 100, 200, 500,$ and 1000 nm, respectively, Eq. (16) predicts the dimensionless axial tensile stress σ/μ as shown in Fig. 4. By common sense, the axial stress increases with increasing axial stretch. In addition, Fig. 4 also indicates that l_0 has increasing influence on the stress variation with increasing amplitude of l_0 , which demonstrates the strong size effect in soft rubbery nanofibers. In the particular case of $l_0 = 1000$ as shown in Fig. 4(d), the soft nanofiber with the diameter of 50 nm exhibits longitudinal elastic instability.

B. Critical condition of circumferential wrinkling in soft polymer nanofibers

Equation (36) indicates that the critical condition of surface wrinkling is $B = 0$, which results in the critical axial stretch as

$$\lambda_3 = \left(4 \frac{R_0}{l_0}\right)^{2/3}. \quad (38)$$

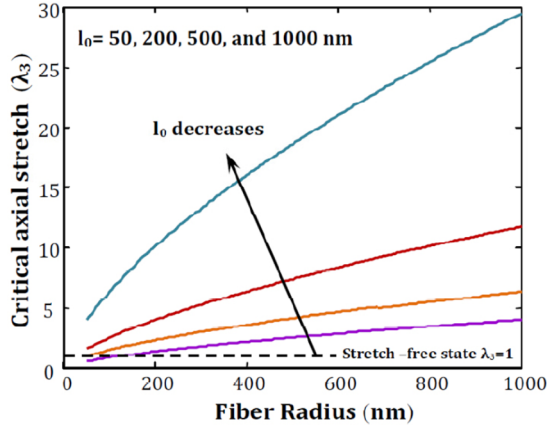


FIG. 5. Variation of the critical axial stretch λ_3 with respect to varying fiber radius R at four different intrinsic lengths ($l_0 = 50, 200, 500, \text{ and } 1000 \text{ nm}$, respectively) based on relation (40).

Yet, it needs to be mentioned that this critical stretch λ_3 only corresponds to $k = 0$, i.e., a mathematical critical condition for surface instability (wrinkling). For those physically meaningful wave numbers $k > 0$, $k = 1$ corresponds to a circular cross-sectional configuration; $k = 2$ corresponds to an elliptic cross-sectional configuration. Thus, it is reasonable to assume that the critical stretch λ_3 is the one that triggers the first physically meaningful wrinkle mode with $k = 2$, i.e.,

$$k = \sqrt{B/A} = 2. \quad (39)$$

Plugging (30) and (31) into (40) results in

$$\lambda_3 = 4 \left(\frac{R_0}{l_0} \right)^{2/3}, \quad (40)$$

which is $4^{1/3} \approx 1.5874$ times the one predicted by relation (38).

Figure 5 illustrates the critical axial stretch λ_3 based on relation (40) with increasing initial fiber radius R_0 at four intrinsic lengths of $l_0 = 50, 200, 500, \text{ and } 1000 \text{ nm}$, respectively. Given the value of R_0 , the critical axial stretch λ_3 decreases rapidly with increasing l_0 ; i.e., the size effect is significant enough in the critical axial stretch λ_3 to trigger circumferential wrinkling. More noticeably, at the small nanofiber sizes a large intrinsic length l_0 may evoke spontaneous wrinkling; i.e., surface circumferential wrinkling may be directly evoked by surface energy without axial stretching and even under axial compression ($\lambda_3 < 1$).

C. Critical radii for circumferential wrinkling in soft polymer nanofibers

Relation (40) can further determine the critical fiber radius R_C to trigger circumferential wrinkling ($k = 2$) at the stretch-free condition, i.e., $\lambda_3 = 1$, such that

$$R_C = \frac{\gamma}{8c_1}. \quad (41)$$

Relation (41) indicates that circumferential wrinkling of soft polymer nanofibers may happen without applying any

axial tensile stretch, i.e., spontaneous circumferential wrinkling, if the initial fiber radius is smaller than the critical fiber radius R_C as also shown in Fig. 5. This critical fiber radius R_C depends only on the surface energy and elastic properties of the soft nanofibers, and is irrelevant to the material and process parameters adopted in an electrospinning process. In addition, by comparison with R_C to trigger spontaneous longitudinal wrinkling in soft nanofibers as studied by Wu [61] and Wu *et al.* [62], i.e., $R_C = (\gamma/\mu)/12$ after converting into the current neo-Hookean material model, it is found that R_C to trigger spontaneous circumferential wrinkling is 1.5 times that to trigger spontaneous longitudinal wrinkling. This demonstrates that spontaneous circumferential wrinkling occurs earlier than spontaneous longitudinal wrinkling in electrospun nanofibers as the electrospinning jet is shrinking from a larger size to a smaller one and wrinkling, satisfying the critical condition at which a large fiber radius first occurs. Thus, spontaneous circumferential wrinkles can be observed more often in electrospun soft nanofibers, which has been broadly validated in electrospinning experiments with one sample as shown in Fig. 1.

D. Wave number (wrinkle mode) for circumferential wrinkling in soft polymer nanofibers

Substitution of Eqs. (30) and (31) into (35) leads to the wave number k (wrinkle mode) of a soft nanofiber as

$$k = \sqrt{-4 + \frac{l_0}{R_0} \lambda_3^{3/2}}. \quad (42)$$

Figure 6 shows the numerical scaling analysis of the dependencies of the wave number k upon the axial stretch λ_3 at four initial fiber radii R_0 and four intrinsic lengths l_0 as adopted in Sec. II A, respectively. Herein, wave numbers $k = 1$ and 2 correspond to the circular and elliptical nanofiber cross sections, respectively. The physically meaningful wrinkle modes can be considered for those with wave numbers $k \geq 2$.

Figure 6 shows variations of the wave number k (wrinkle mode) of soft nanofibers with respect to varying axial stretch λ_3 at four different initial fiber radii R_0 and four intrinsic lengths l_0 , respectively. Given the values of R_0 and l_0 , k increases in a slightly nonlinear feature with increasing λ_3 . In addition, at a fixed value of λ_3 , k increases with either increasing l_0 or decreasing R_0 , i.e., the smaller the soft nanofiber radii, the more the circumferential surface wrinkles appear. Figure 6 also indicates that axial stretching can be utilized to tune the circumferential wrinkling in soft nanofibers and then rationally modify the surface morphology and specific surface area of the soft nanofibers for promising applications in gas and liquid filtration, water-oil separation, biological tissue scaffolding, etc. In principle, surface morphology can be actively altered to optimize the surface wetting performance of nanofiber mats [11] according to the Wenzel and the Cassie and Baxter models for patterned superhydrophobic surfaces [78–80].

Nevertheless, substantial experimental data are still desired for surface energy, mechanical properties, and drying induced residual strains across the electrospun polymer nanofibers. Thus, quantitative model validation is still pending at this

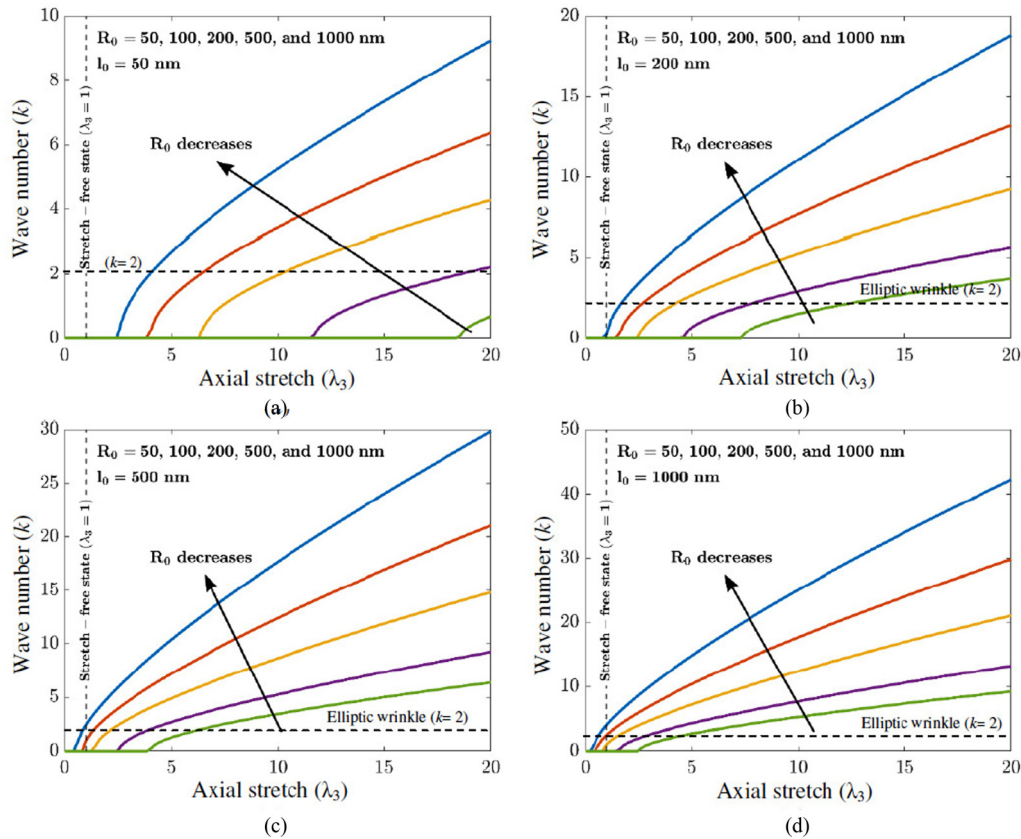


FIG. 6. Variation of the wave number k (wrinkle mode) of soft nanofibers with respect to varying axial stretch λ_3 at four different initial fiber radii R_0 and four intrinsic lengths l_0 (R_0 and $l_0 = 50, 200, 500$, and 1000 nm, respectively).

stage though the present model is able to qualitatively predict the existence of circumferential wrinkling and to indicate the crucial role of surface energy in dominating the surface wrinkling phenomenon in electrospun polymer nanofibers. Additional model refinements and validation are expected once sufficient experimental data of soft polymer nanofibers are available.

IV. CONCLUDING REMARKS

In this study, the mechanism of circumferential surface wrinkling of soft polymer nanofibers under axial stretching has been explored via forming a simple one-dimensional (1D) nonlinear elastic model. During the process, the possible processing-induced radial gradients of the mechanical properties in the fiber cross section were ignored, and the material of the soft polymer nanofibers was assumed to be a homogeneous, isotropic, hyperelastic neo-Hookean solid. The governing ODE for circumferential wrinkling has been

determined. The critical axial stretch to trigger circumferential wrinkling and the critical initial fiber radius to evoke spontaneous circumferential wrinkling have been extracted in explicit expressions. Detailed numerical scaling analysis has been performed to illustrate the dependencies of critical axial stretch and critical fiber radius upon the material properties and geometries of the soft nanofibers. The present study provides the rational basis of the circumferential wrinkling phenomenon commonly observed in soft polymer nanofibers produced by electrospinning. The study also demonstrates a potential technique to actively tune the surface morphology of soft polymer nanofibers via axial stretching to induce circumferential wrinkling.

ACKNOWLEDGMENTS

Partial support of this work by the NSF (Award No.: CMMI-1234297), DOE, and NDSU Development Foundation (Awards No. FAR0021589 and No. FAR0031220) is gratefully appreciated.

- [1] D. H. Reneker and I. Chun, *Nanotechnology* **7**, 216 (1996).
- [2] Y. Dzenis, *Science* **304**, 1917 (2004).
- [3] D. Li and Y. N. Xia, *Adv. Mater.* **16**, 1151 (2004).
- [4] D. H. Reneker and A. L. Yarin, *Polymer* **49**2387 (2008).

- [5] P. Gibson, H. Schreuder-Gibson, and D. Rivin, *Colloids Surf., A* **187**, 469 (2001).
- [6] D. Smith, D. H. Reneker, W. Kataphinan, and A. Dabney, US Patent No. 6,821,479 (2001).

- [7] D. Smith and D. H. Reneker, US Patent No. 6,753,454 (2004).
- [8] R. Gopal, S. Kaur, Z. W. Ma, C. Chan, S. Ramakrishna, and T. Matsuura, *J. Membr. Sci.* **281**, 581 (2006).
- [9] B. Maze, H. V. Tafreshi, Q. Wang, and B. Pourdeyhimi, *J. Aerosol Sci.* **38**, 550 (2007).
- [10] R. S. Barhate and S. Ramakrishna, *J. Membr. Sci.* **296**, 1 (2007).
- [11] Z. Zhou and X. F. Wu, *Mater. Lett.* **160**, 423 (2015).
- [12] Z. Zhou, W. Lin, and X. F. Wu, *Colloids Surf., A* **494**, 21 (2016).
- [13] J. S. Kim and D. H. Reneker, *Polym. Compos.* **20**, 124 (1999).
- [14] Z. M. Huang, Y. Z. Zhang, M. Kotaki, and S. Ramakrishna, *Compos. Sci. Technol.* **63**, 2223 (2003).
- [15] Y. Dzenis, *Science* **319**, 419 (2008).
- [16] X. F. Wu, *Fracture of Advanced Polymer Composites with Nanofiber Reinforced Interfaces: Fabrication, Characterization and Modeling* (VDM Verlag, Düsseldorf, Germany, 2009).
- [17] Q. Chen, L. Zhang, A. Rahman, Z. Zhou, X. F. Wu, and H. Fong, *Composites, Part A* **42**, 2036 (2011).
- [18] X. F. Wu, A. Rahman, Z. P. Zhou, D. D. Pelot, S. Sinha-Ray, B. Chen, S. Payne, and A. L. Yarin, *J. Appl. Polym. Sci.* **129**, 1383 (2013).
- [19] X. F. Wu and Y. A. Yarin, *J. Appl. Polym. Sci.* **130**, 2225 (2013).
- [20] W. J. Li, C. T. Laurencin, E. J. Caterson, R. S. Tuan, and F. K. Ko, *J. Biomed. Mater. Res.* **60**, 613 (2002).
- [21] J. A. Matthews, G. E. Wnek, D. G. Simpson, and G. L. Bowlin, *Biomacromolecules* **3**, 232 (2002).
- [22] C. Burger, B. S. Hsiao, and B. Chu, *Annu. Rev. Mater. Res.* **36**, 333 (2006).
- [23] S. P. Pham, U. Sharma, and A. G. Mikos, *Tissue Eng.* **12**, 1197 (2006).
- [24] E. R. Kenawy, G. L. Bowlin, K. Mansfield, J. Layman, D. G. Simpson, E. H. Sanders, and G. E. Wnek, *J. Controlled Release* **81**, 57 (2002).
- [25] S. Y. Chew, Y. Wen, Y. Dzenis, and K. W. Leong, *Curr. Pharm. Des.* **12**, 4751 (2006).
- [26] D. Liang, B. S. Hsiao, and B. Chu, *Adv. Drug Delivery Rev.* **59**, 1392 (2007).
- [27] C. P. Barnes, S. A. Sell, E. D. Boland, D. G. Simpson, and G. L. Bowlin, *Adv. Drug Delivery Rev.* **59**, 1413 (2007).
- [28] J. W. Xie, X. R. Li, and Y. N. Xia, *Micromol. Rapid Commun.* **29**, 1775 (2008).
- [29] C. Kim, B. T. N. Ngoc, K. S. Yang, M. Kojima, Y. A. Kim, Y. J. Kim, M. Endo, and S. C. Yang, *Adv. Mater.* **19**, 2341 (2007).
- [30] L. W. Ji and X. W. Zhang, *Carbon* **47**, 3219 (2009).
- [31] D. L. Schulz, J. Hoey, J. Smith, A. Elangovan, X. Wu, I. Akhatov, S. Payne, J. Moore, P. Boudjouk, L. Pederson, J. Xiao, and J. G. Zhang, *Electrochem. Solid State Lett.* **13**, A143 (2010).
- [32] Z. X. Dong, S. J. Kennedy, and Y. Q. Wu, *J. Power Sources* **196**, 4886 (2011); X. W. Zhang, L. W. Ji, O. Toprakci, Y. Z. Liang, and M. Alcoutlabi, *Polym. Rev.* **51**, 239 (2011).
- [33] P. Joshi, Z. P. Zhou, P. Poudel, A. Thapa, X. F. Wu, and Q. Q. Qiao, *Nanoscale* **4**, 5659 (2012); Z. Zhou, X. F. Wu, and H. Fong, *Appl. Phys. Lett.* **100**, 023115 (2012).
- [34] Z. Zhou and X. F. Wu, *J. Power Sources* **222**, 410 (2013); **262**, 44 (2014).
- [35] Z. Zhou, X. F. Wu, and H. Hou, *RSC Adv.* **4**, 23622 (2014).
- [36] D. H. Reneker, A. L. Yarin, E. Zussman, and H. Xu, *Adv. Appl. Mech.* **41**, 43 (2007).
- [37] V. N. Kirichenko, I. V. Petryanov-Sokolov, N. N. Suprun, and A. A. Shutov, *Sov. Phys. - Dokl.* **31**, 611 (1986).
- [38] D. A. Saville, *Annu. Rev. Fluid Mech.* **29**, 27 (1997).
- [39] A. F. Spivak and Y. A. Dzenis, *Appl. Phys. Lett.* **73**, 3067, (1998).
- [40] A. F. Spivak, Y. A. Dzenis, and D. H. Reneker, *Mech. Res. Commun.* **27**, 37 (2000).
- [41] J. J. Feng, *J. Non-Newtonian Fluid Mech.* **116**, 55 (2003).
- [42] J. J. Feng, *Phys. Fluids* **14**, 3912 (2002).
- [43] X. F. Wu, Z. Zhou, O. Zholobko, J. J. Jenniges, B. Baatz, M. Ahmadi, and J. Chen, *J. Appl. Phys.* **127**, 054303, 2020.
- [44] S. Cuenot, S. Demoustier-Champagne, and B. Nysten, *Phys. Rev. Lett.* **85**, 1690 (2000).
- [45] E. P. S. Tan and C. T. Lim, *Rev. Sci. Instrum.* **75**, 2581 (2004).
- [46] E. P. S. Tan, C. N. Goh, C. H. Sow, and C. T. Lim, *Appl. Phys. Lett.* **86**, 073115 (2005).
- [47] E. P. S. Tan, S. Y. Ng, and C. T. Lim, *Biomaterials* **26**, 1453 (2005).
- [48] R. Inai, M. Kotaki, and S. Ramakrishna, *Nanotechnology* **16**, 208 (2005).
- [49] E. P. S. Tan and C. T. Lim, *Compos. Sci. Technol.* **66**, 1102 (2006).
- [50] Y. Ji, B. Q. Li, S. R. Ge, J. C. Sokolov, and M. H. Rafailovich, *Langmuir* **22**, 1321 (2006).
- [51] E. Zussman, M. Burman, A. L. Yarin, R. Khalfin, and Y. Cohen, *J. Polym. Sci., Part B: Polym. Phys.* **44**, 1482 (2006).
- [52] P. A. Yuya, Y. K. Wen, J. A. Turner, Y. A. Dzenis, and Z. Li, *Appl. Phys. Lett.* **90**, 111909 (2007).
- [53] A. Arinstein, M. Burman, O. Gendelman, and E. Zussman, *Nat. Nanotechnol.* **2**, 59 (2007).
- [54] M. Naraghi, I. Chasiotis, H. Kahn, Y. K. Wen, and Y. Dzenis, *Appl. Phys. Lett.* **91**, 151901 (2007).
- [55] M. Naraghi, I. Chasiotis, H. Kahn, Y. Wen, and Y. Dzenis, *Rev. Sci. Instrum.* **78**, 085108 (2007).
- [56] X. F. Wu and Y. A. Dzenis, *J. Appl. Phys.* **98**, 093501 (2005).
- [57] X. F. Wu and Y. A. Dzenis, *J. Appl. Phys.* **100**, 124318 (2006).
- [58] X. F. Wu and Y. A. Dzenis, *J. Appl. Phys.* **102**, 044306 (2007).
- [59] X. F. Wu and Y. A. Dzenis, *J. Phys. D: Appl. Phys.* **40**, 4276 (2007).
- [60] X. F. Wu and Y. A. Dzenis, *Nanotechnology* **18**, 285702 (2007).
- [61] X. F. Wu, Y. Y. Kostogorova-Beller, A. V. Goponenko, H. Q. Hou, and Y. A. Dzenis, *Phys. Rev. E* **78**, 061804 (2008).
- [62] X. F. Wu, *J. Appl. Phys.* **107**, 013509 (2010).
- [63] X. F. Wu, A. Bedarkar, and I. S. Akhatov, *J. Appl. Phys.* **108**, 083518 (2010).
- [64] X. F. Wu, Z. P. Zhou, and W. M. Zhou, *Appl. Phys. Lett.* **100**, 193115 (2012).
- [65] A. L. Yarin, S. Koombhongse, and D. H. Reneker, *J. Appl. Phys.* **90**, 4836 (2001); G. Taylor, *Proc. R. Soc. London, Ser. A* **313**, 453 (1969).
- [66] D. H. Reneker, A. L. Yarin, H. Fong, and S. Koombhongse, *J. Appl. Phys.* **87**, 4531 (2000).
- [67] A. L. Yarin, S. Koombhongse, and D. H. Reneker, *J. Appl. Phys.* **89**, 3018 (2001).
- [68] Y. M. Shin, M. M. Hohman, M. P. Brenner, and G. C. Rutledge, *Appl. Phys. Lett.* **78**, 1149 (2001).
- [69] M. M. Hohman, M. Shin, G. Rutledge, and M. P. Brenner, *Phys. Fluids* **13**, 2221 (2001).
- [70] X. F. Wu, Y. Salkovskiy, and Y. A. Dzenis, *Appl. Phys. Lett.* **98**, 223108 (2011).

- [71] S. Koombhongse, W. Liu, and D. H. Reneker, *J. Polym. Sci., Part B: Polym. Phys.* **39**, 2598 (2001).
- [72] S. Mora, T. Phou, J.-M. Fromental, L. M. Pismen, and Y. Pomeau, *Phys. Rev. Lett.* **105**, 214301 (2010).
- [73] M. Taffetani and P. Ciarletta, *Phys. Rev. E* **91**, 032413 (2015).
- [74] M. Taffetani and P. Ciarletta, *J. Mech. Phys. Solids* **81**, 91 (2015).
- [75] P. Ciarletta, D. Destrade, A. L. Gower, and M. Taffetani, *J. Mech. Phys. Solids* **90**, 242 (2016).
- [76] C. L. Pai, M. C. Boyce, and G. C. Rutledge, *Macromolecules* **42**, 2102 (2009).
- [77] M. Ahmadi and X. F. Wu, *J. Phys. Commun.* **3**, 045001 (2019).
- [78] R. N. Wenzel, *Ind. Eng. Chem.* **28**, 988 (1936).
- [79] R. N. Wenzel, *J. Phys. Colloid Chem.* **53**, 1466 (1949).
- [80] A. B. D. Cassie and S. Baxter, *Trans. Faraday Soc.* **40**, 546 (1944).